Supplementary Information (SI) for Journal of Materials Chemistry A.
This journal is © The Royal Society of Chemistry 2026

Defect Engineering in Carbon Skeletons toward Precise Edge-Nitrogen Doping for Efficient Electrochemical Energy Storage

Yi Yang*, Qiu-xiang Chen, Xing-yue Huang, Huan Liu, Tian Xia, You-bing Li, Jin-yong Mo*

College of Materials Science and Engineering, Chongqing University of Technology, Chongqing, People's Republic of China

*E-mail: yiyang@cqut.edu.cn; jinyong@cqut.edu.cn

Calculation of capacitive contribution

The potential-dependent current of an electrode typically consists of two components: a capacitive contribution and a diffusion-controlled one. The capacitive response is rapid and originates from electric double-layer charging and surface-confined Faradaic reactions occurring within a shallow region of the electrode. In contrast, the diffusion-controlled contribution stems from bulk Faradaic processes governed by the diffusion of electroactive species inside the electrode. To further clarify the charge-storage kinetics, the power-law relationship and Dunn's method are used.

The power-law relationship: The current response from a cyclic voltammogram obeys the relationship of Equation S1

$$i = av^b \qquad \text{(S1)}$$

Where a and b are adjustable parameters. For the ideal capacitive behavior, the current response is proportional to the scan rate (b=1). The current response of diffusion-limited process is proportional to the square root of the scan rate (b=0.5). The adjustable parameters of a and b can be calculated using the linear fitting of lg$i$ and lg$v$ with the following Equation S2.

$$lgi=lga+blgv \qquad \text{(S2)}$$

Dunn's method: At a given potential, the total current response (i) can be quantitatively separated into these two components using the following expression:

$$i = k_1v + k_2v^{1/2} \qquad \text{(S3)}$$

Where k_1v originates from the capacitive contribution, $k_2v^{1/2}$ originates from the

diffusion-limited Faradaic processes. By rearranging the above equation into the following Equation S4, the two components can be effectively decoupled based on the linear relationship between $i/v^{1/2}$ and $v^{1/2}$.

$$i/v^{1/2} = k_1 v^{1/2} + k_2 \qquad \text{(S4)}$$

From the slope and intercept of this linear fit, the constants k_1 and k_2 can be determined, enabling the quantitative estimation of the current contributions from capacitive and diffusion-controlled processes.

Supplementary tables and Figures

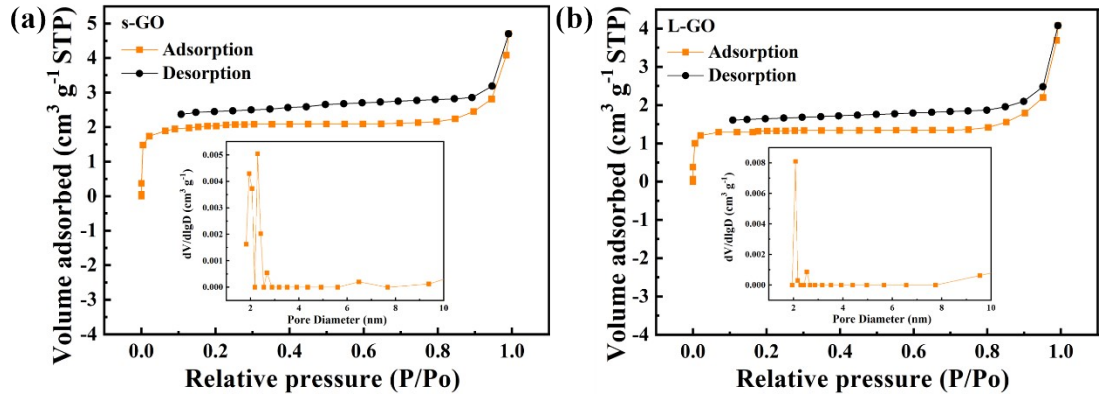

Fig. S1 Nitrogen adsorption-desorption isotherm of (a) s-GO and (b) L-GO. The inset shows the corresponding pore size distribution (BJH)

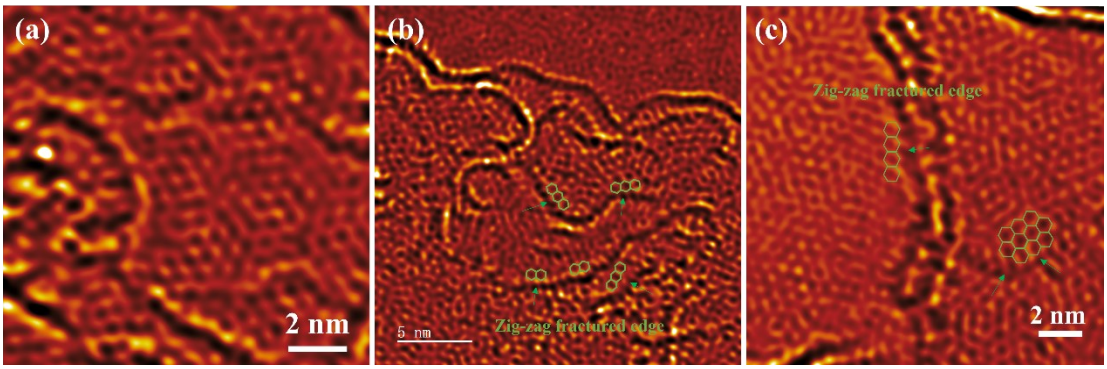

Fig. S2 AC-TEM images of s-GO carbon frameworks. (a) A clear version without annotations of the image shown in Fig. 2f. (b, c) AC-TEM images of different regions. The structure exhibited numerous crack boundaries and clearly defined zigzag carbon edges after ultrasonic treatment.

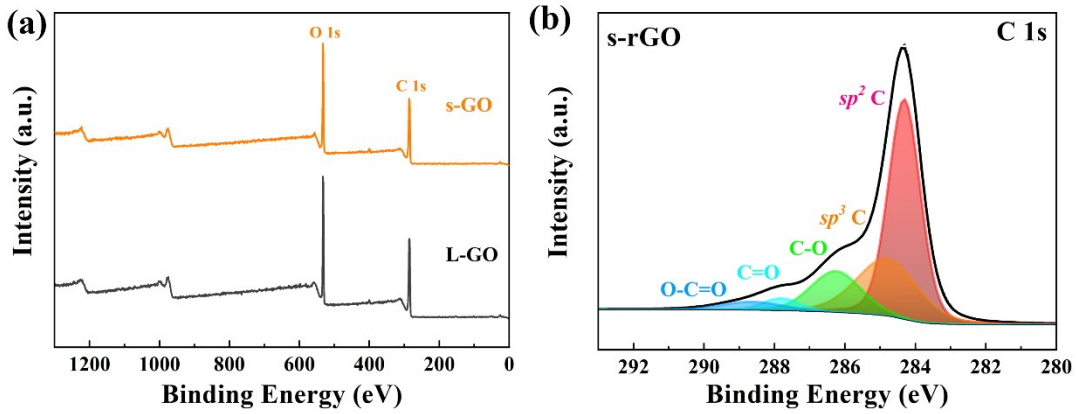

Fig. S3 (a) Full XPS spectra of s-GO and L-GO, displaying prominent peaks for oxygen (O 1s) and carbon (C 1s). (b) High-resolution XPS C 1s spectra of s-rGO.

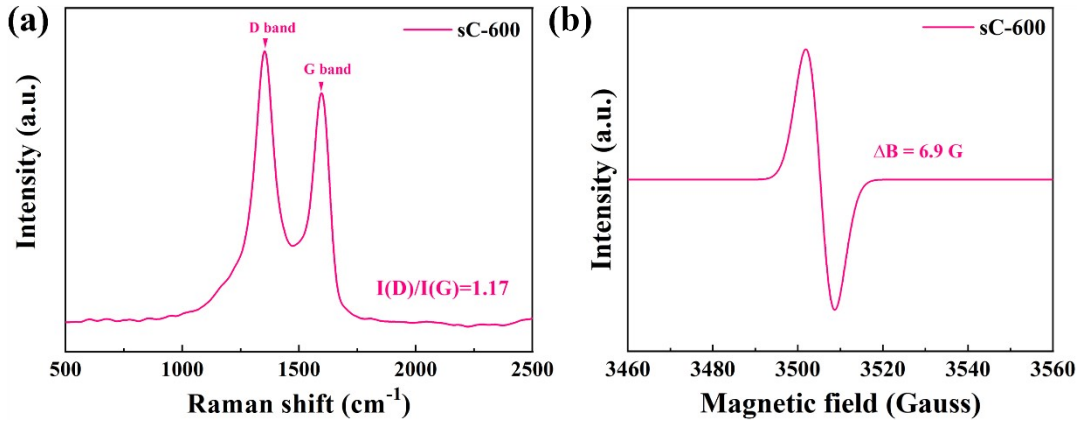

Fig. S4 (a) Raman and (b) EPR spectra of sC-600.

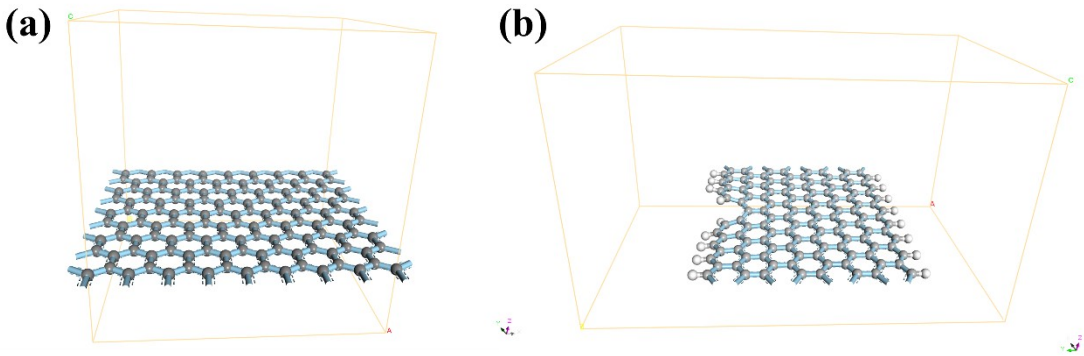

Fig. S5 The prototypical carbon skeleton models based on the graphene structure. (a) Boundary-free monolayer graphene. (b) Zigzag graphene nanoribbon (GNR) consisting of eight carbon atom rows terminated by hydrogen atoms, containing a carbon vacancy located at a zigzag edge.

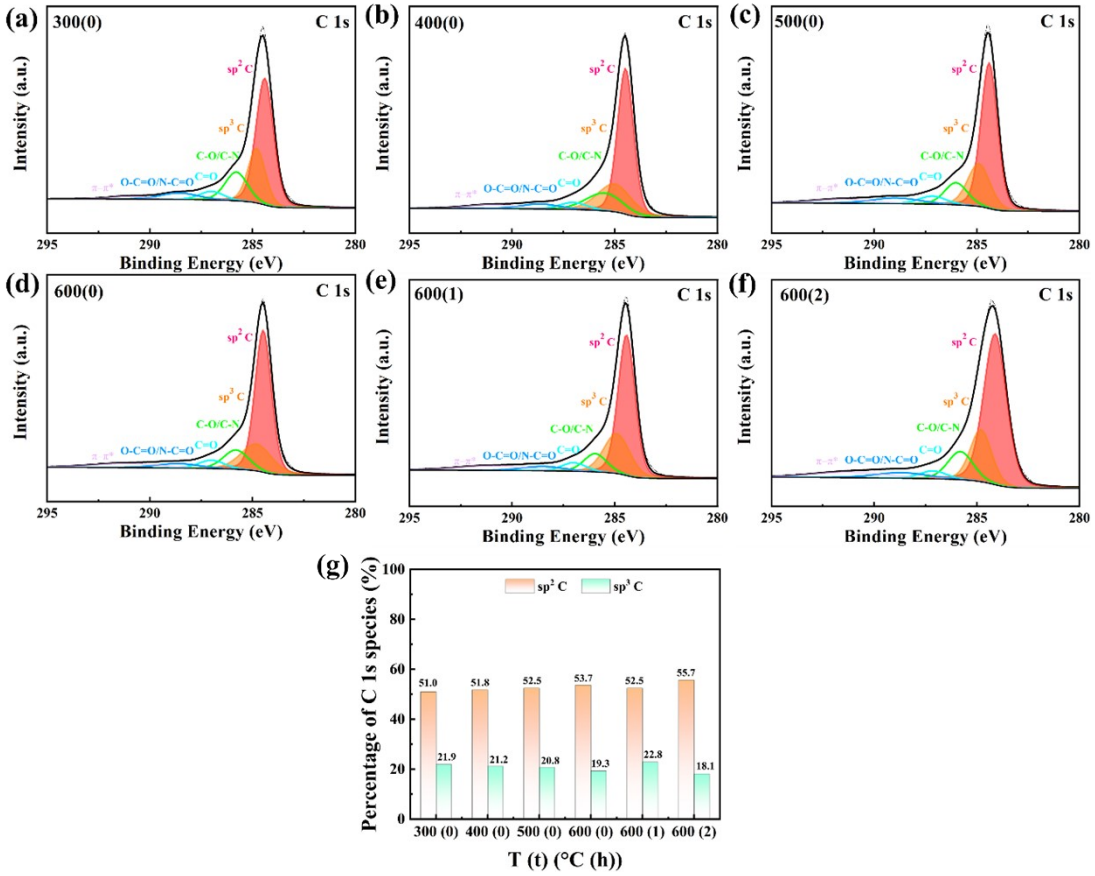

Fig. S6 High-resolution XPS C 1s spectra of s-rGO treated at (a) 300 °C, (b) 400 °C, (c) 500 °C, (d) 600 °C, (e) 600 °C for 1 h and (f) 600 °C for 2 h (sN-C-600). (g) Percentage of sp^2 C and sp^3 C in above samples.

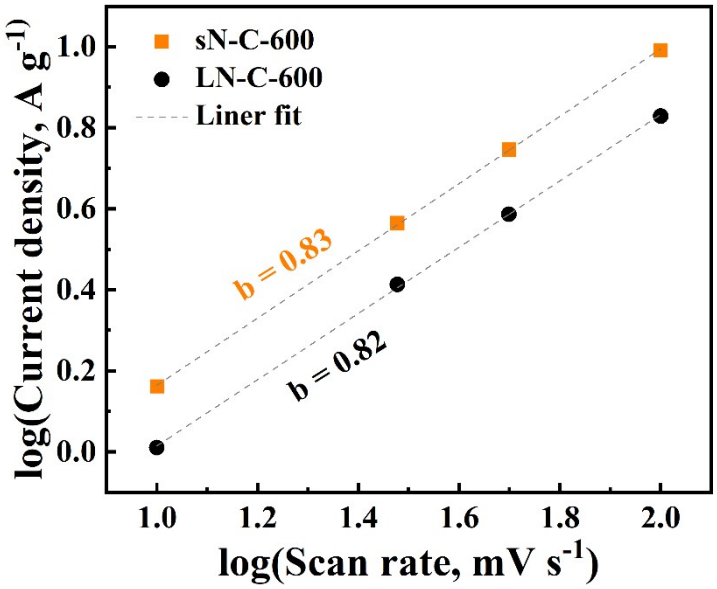

Fig. S7 Logarithmic plots of cathodic peak current density versus scan rate, and the corresponding b-values for sN-C-600 and LN-C-600 determined via the power-law relationship.

Table S1 Pore parameters of s-GO and L-GO.

Samples	Specific surface area (BET, $m^2 g^{-1}$)	Average pore diameter (BJH, nm)	Pore volume ($cm^3 g^{-1}$)
s-GO	7.75	**13.01**	0.0071
L-GO	5.25	**20.45**	0.0060

Table S2 Pore size distribution of s-GO and L-GO.

Pore Classification	Pore size distribution (nm)	Specific surface area ($m^2 g^{-1}$)	
		s-GO	**L-GO**
Micropores (T-plot)	0.35-2	**7.670**	5.204
Mesopores (BJH)	2-10	**0.936**	0.375
	10-50	**0.453**	0.492
Macropores (BJH)	50-196	**0.026**	0.013

Table S3 Atomic percentages (at. %) of C and O in s-GO and L-GO, with proportions of different C 1s species.

Samples	C (at. %)	O (at. %)	C/O	C 1s species (%)				
				sp^2 C	sp^3 C	C-O	C=O	O-C=O
s-GO	67.4	32.6	**2.07**	**29.2**	17.6	40.7	7.9	4.6
L-GO	67.6	32.4	**2.09**	**35.4**	12.9	40.1	7.6	4.0

Table S4 Atomic percentages (at. %) of C and O in s-rGO, with proportions of different C 1s species.

Samples	C (at. %)	O (at. %)	C/O	C 1s species (%)				
				sp^2 C	sp^3 C	C-O	C=O	O-C=O
s-rGO	81.7	18.3	**4.46**	**51.6**	25.9	15.2	3.4	3.9

Table S5 Proportions of different N 1s configurations in sN-C-Ts and LN-C-Ts (500-900).

Samples	N Configurations (%)				
	N-6	N-5	Edge-N	N-Q	Oxidic-N
sN-C-500	40.7	30.4	**71.1**	16.8	12.1
LN-C-500	44.2	27.4	**71.6**	14.2	14.2
sN-C-600	47.3	24.5	**71.8**	18.7	9.5
LN-C-600	29.2	33.6	**62.8**	27.5	9.6
sN-C-700	35.9	25.8	**61.7**	19.5	18.8
LN-C-700	18.0	39.7	**57.7**	36.4	5.9
sN-C-800	28.5	28.1	**56.6**	30.0	13.3
LN-C-800	21.7	29.3	**51**	37.3	11.7
sN-C-900	33.3	22.9	**56.2**	31.2	12.6
LN-C-900	25.1	25.0	**50.1**	36.4	13.5

Table S6 Atomic percentages (at. %) of C, O and N in sN-C-Ts (500-900).

Samples	C (at. %)	O (at. %)	N (at. %)	N/C (%)
sN-C-500	89.2	5.2	**5.6**	**6.3**
sN-C-600	89.0	4.7	**6.3**	**7.1**
sN-C-700	92.7	3.5	**3.8**	**4.1**
sN-C-800	93.2	3.3	**3.5**	**3.8**

sN-C-900	95.2	2.5	**2.3**	**2.4**

Table S7 Relative proportions of N species (including N-6, N-5, N-Q and Oxidic-N) and π*/σ* ratios for the edge and basal plane regions of sN-C-600.

	π* States (%)					**π*/σ***
	N-6	**N-5**	Edge-N	**N-Q**	**Oxidic-N**	
sN-C-600: Edge	**39.0**	**11.3**	50.3	**16.0**	**33.7**	**4.1**
sN-C-600: In-plane	**7.5**	**23.2**	30.7	**11.1**	**58.2**	**0.5**

Table S8 Atomic percentages (at. %) of C, O and N, and relative proportions of nitrogen configuration (including N-6, N-5, N-Q and Oxidic-N) in the samples of s-rGO treated at 300 °C, 400 °C, 500 °C, 600 °C, 600 °C for 1 h and 600 °C for 2 h (sN-C-600).

T (t) /°C (h)	**C (at. %)**	**O (at. %)**	**N (at. %)**	**N/C**	**N Configuration (%)**					**N-6/ N-5**
					N-6	**N-5**	**Edge-N**	**N-Q**	**Oxidic-N**	
300 (0)	87.4	9.6	3.0	**3.4%**	35.6	37.7	**73.3**	14	12.8	**94.4%**
400 (0)	87.8	9.0	3.2	**3.6%**	44.2	29.6	**73.8**	14.6	11.7	**149.3%**
500 (0)	89.6	6.8	3.6	**4.0%**	45.0	26.9	**71.9**	14	14.1	**167.3%**
600 (0)	89.7	6.3	4.0	**4.4%**	46.1	25.3	**71.4**	14.3	14.2	**182.2%**
600 (1)	89.4	5.7	4.9	**5.5%**	48.6	25.8	**74.4**	12.6	12.9	**188.4%**
600 (2)	89.0	4.7	6.3	**7.1%**	47.3	24.5	**71.8**	18.7	9.5	**193.1%**

Table S9 relative proportions of C 1s species (including sp^2 C, sp^3 C, C-O/C-N, C=O, O-C=O/N-C=O and π–π*) in the samples of s-rGO treated at 300 °C, 400 °C, 500 °C, 600 °C, 600 °C for 1 h and 600 °C for 2 h (sN-C-600).

Samples	C 1s Species (%)					
	sp^2 C	**sp^3 C**	**C-O/C-N**	**C=O**	**O-C=O/ N-C=O**	**π–π***
300(0)	**51.0%**	**21.9%**	14.5%	4.6%	5.5%	2.5%
400(0)	**51.8%**	**21.2%**	14.4%	4.2%	4.3%	4.1%
500(0)	**52.5%**	**20.8%**	10.8%	4.7%	5.9%	5.3%
600(0)	**53.7%**	**19.3%**	11.0%	4.8%	4.3%	6.8%
600(1)	**52.5%**	**22.8%**	9.1%	4.5%	4.0%	7.1%
600(2)	**55.7%**	**18.1%**	11.4%	3.4%	4.7%	6.7%